

RESEARCH PAPER

Synthesis, characterization and catalytic activity of co-polymer hydrogels based on (3-acrylamidopropyl) trimethyl ammonium chloride and acrylonitrile, a reusable nanocatalyst

Zahra Mohammadi, Massomeh Ghorbanloo*, Tahere Mokary-Yazdely

Department of Chemistry, Faculty of Science, University of Zanjan, Iran

ARTICLE INFO

Article History:

Received 19 May 2020

Accepted 08 September 2020

Published 15 October 2020

Keywords:

Co-polymer

Acrylonitrile

Cationic hydrogels

Reusable; Nanocomposites

ABSTRACT

Cationic poly(acrylonitril-co-acrylamidopropyl-trimethyl ammonium chloride) (p(AN-co-APTMACI)) hydrogels in bulk were synthesized using acrylonitrile (AN) and 3-acrylamidopropyl-trimethyl ammonium chloride (APTMACI) as monomers. The chemical structure of the synthesized (p(AN-co-APTMACI)) macroporous hydrogel was confirmed by Fourier transform infrared (FT-IR), and scanning electron microscopy (SEM). P(AN-co-APTMACI) was successfully utilized for the in situ synthesis and stabilization of silver nanoparticles within the hydrogel matrix. These hydrogel composites were characterized by FT-IR, and field-emission SEM, transmission electron microscopy, and atomic absorption spectroscopy. The morphology of p(AN-co-APTMACI) reveals the formation of homogeneous and highly porous material. Catalytic activity of p(AN-co-APTMACI)-Ag catalyst was investigated in the aerobic oxidation of olefins, reduction of 4-nitrophenol and hydrolysis of sodium borohydride by the emphasis on the effects of different parameters such as temperature, substituent effect, etc. The catalyst was easily recovered from the reaction medium and it could be re-used for other five runs without significant loss of activity.

How to cite this article

Mohammadi Z., Ghorbanloo M., Mokary-Yazdely T. Synthesis, characterization and catalytic activity of co-polymer hydrogels based on (3-acrylamidopropyl) trimethyl ammonium chloride and acrylonitrile, a reusable nanocatalyst. *Nanochem Res*, 2020; 5(2):211-224. DOI: 10.22036/ncr.2020.02.011

INTRODUCTION

Hydrogels are 3D cross-linked hydrophilic polymers capable to absorb large amount of water and remain insoluble in aqueous solutions [1]. In fact, they are considered as intermediates between liquids and solids [2], they have solid-like mechanical performance as well as liquid-like diffusion properties. Due to the large swelling in water, high aqueous content, biocompatibility and low toxicity, hydrogels have been used as a polymeric matrix in formation of nanocomposites using metallic nanoparticles [3], and absorbent pads and numerous biomedical applications [4]. Depending on the nature of the polymeric network, hydrogels could show changes in their dynamic properties varying the external conditions

such as pH, temperature, and ionic strength [5]. In addition, improving the properties of hydrogels through addition of multiple functionalities by the incorporation of different entities into hydrogels, via physical blending or interpenetrating network structure or polymeric composite formation, is possible [6].

In recent decades, a noteworthy attempt has been made on preparation and study of metal particles on the nanometer scales due to their unique physical and chemical properties. It has been known that silver and its compounds have strong inhibitory and bactericidal effects. Currently, hydrogel materials containing Ag in the form of nanoparticles (NP) are receiving increasing attention. The Ag NPs have been incorporated into 3D hydrogel systems to impart mechanical or functional properties [7-

* Corresponding Author Email: m_ghorbanloo@znu.ac.ir

9]. The good reducibility and protective ability of the hydrogels have been advantageous in the green and cost-effective syntheses of NPs [10]. The free-space between the networks in the swollen stage serves as a site for nucleation and growth of Ag NPs and the gel network acts as a nanoreactor or a nanopot. The 3D network prevents aggregation and guarantees mass transport, so enhancing performance by offsetting the main disadvantage of nanoparticles in practical application [11]. The growth and anchoring of inorganic nanomaterials with a high loading amount occur, because of high specific surface area and porosity of 3D networks. Subsequently, the synergistic effect of the two components will be largely enhanced. Recently Ag nano hydrogels of biopolymers have been widely explored as drug delivery systems [12], scaffolds [13,14], and biosensors [15] in photonics [16].

Herein, acrylonitrile (AN) and 3-acrylamidopropyl-trimethyl ammonium chloride (APTMA-Cl) monomers were used for co-polymeric hydrogel preparation. AN is typically a kind of hydrophobic monomer, and it cannot be directly utilized to fabricate PAN-based hydrogels in pure water [17]. P(APTMA-Cl) is an attractive cationic smart material possessing quaternary ammonium salt which renders a natural positive charge on the polymer chains [18]. Therefore, p(AN-co-APTMA-Cl) hydrogels, containing Ag(I) ions loaded from aqueous media, were prepared. The corresponding metal salt was dissolved in distilled water, put into contact with the cationic hydrogels, and then reduced to Ag metal nano-particles in the presence of NaBH_4 . The prepared metal-containing p(AN-co-APTMA-Cl) demonstrated catalytic performance in aerobic oxidation of olefins, reduction of nitrophenol and NaBH_4 hydrolysis reactions.

EXPERIMENTAL

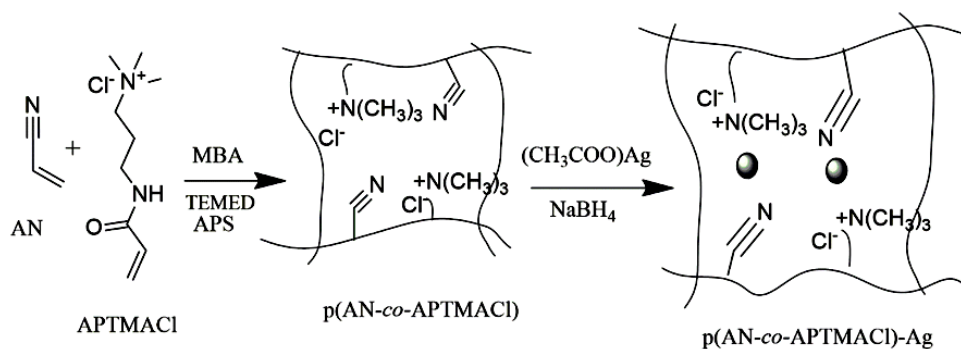
Materials and Equipment

The compounds (3-acrylamidopropyl) trimethyl ammonium chloride (APTMA-Cl) in aqueous solution containing 50 wt% water and acrylonitrile (99%, Sigma Aldrich) as monomers, N,N'-methylenebisacrylamide (MBA) as a crosslinker (99%, Across), ammonium persulfate (APS) as an initiator (99%, Sigma Aldrich) and N,N,N',N'-tetramethylmethylenediamine (TEMED) as an accelerator (98% Across) were used in hydrogel preparation. $\text{Ag}(\text{CH}_3\text{COO})$ (Merck) was used as a metal ion source. Sodium borohydride (NaBH_4 , 98%, Merck) was used in the reduction of

metal ions to prepare metal nanoparticles. FT-IR spectra were recorded in KBr disks with a Bruker FT-IR spectrophotometer. The exact amount of the silver in the composites was determined by AA spectroscopy. The morphology of swollen p(AN-co-APTMA-Cl) hydrogel was investigated with scanning electron microscopy (SEM) via MIRA3 TESCAN FE SEM and an accelerating voltage of 10 keV. The sample was swollen and quickly frozen in liquid nitrogen. The hydrogel was freeze-dried at $-50\text{ }^\circ\text{C}$ for 3 days to preserve their porous structure without any collapse. After that, the dried samples were deposited onto an aluminum stub and sputter-coated with gold for 60 s to enhance conductivity. Transmission electron microscopy (TEM, PHILIPS CM-30) was used to find out the size of metal nanoparticles inside the hydrogel nanocomposites. To image the silver nano particles, TEM analysis was performed on a JEM-2100 (JEOL). The swollen hydrogel was finely grounded using a soft ball, and the resulted hydrogel nanocomposite samples were dispersed in 1 mL of ethanol and dropped on collodion film coated copper grid for TEM analysis. The atomic absorption analysis was carried out using Varian spectra AA 220 equipment. The reduction of nitrophenol was determined using Pharmacia Biotech Ultrospec 4000 UV-Vis spectroscopy. The reaction products of oxidation were determined and analyzed using an HP Agilent 6890 gas chromatograph equipped with a HP-5 capillary column (phenyl methyl siloxane $30\text{ m} \times 320\text{ }\mu\text{m} \times 0.25\text{ }\mu\text{m}$).

Preparation of p(AN-co-APTMA-Cl) hydrogels

The p(AN-co-APTMA-Cl) hydrogel was synthesized via free radical polymerization reaction techniques in mild condition ($30\text{ }^\circ\text{C}$), as shown in Scheme 1 [2]. Briefly, 0.003 g of MBA was dissolved in 0.5 ml (1.6 mmol) AN monomer, and the mixture was added to 1042 ml (1.6 mmol) APTMA-Cl with an equal amount of AN (1:1 mol ratio) and mixed thoroughly. Thereafter, 5 μL TEMED was added to the solution and finally, the initiator solution APS (1 mol% of total monomer) in 100 mL water was added to this hydrogel precursor. After mixing carefully, the solution was injected into plastic straws with 4 mm diameter and allowed to polymerize and crosslink to complete the reaction at ambient temperature. Finally, the obtained 3-D hydrogels were cut in the same shapes, and washed with approximately 2000 mL of water for 24 h. The wash water was



Scheme 1. Schematic representation of synthesis of p(AN-co-APTMACl) composite

replenished every 2 h to remove un-reacted species (monomer, cross-linker, accelerator and initiator). After cleaning the procedure, hydrogels were dried in an oven to a constant weight at 40 °C and kept in sealed containers for further use.

Selected FT-IR (KBr, cm⁻¹): (p(AN-co-APTMACl)): 3479 (br, s), 3292 (sholder), 3072 (w), 3020 (w), 2929 (w), 2878 (w), 2240 (m), 1652 (s), 1552 (m), 1490 (m), 1471 (w), 1394 (w), 1259 (m), 1229 (m), 1124 (m), 966 (m), 959 (w), 706 (w), 619 (w), 534 (w).

In situ synthesis of metal nanoparticles within p(AN-co-APTMACl) hydrogel

For in situ fabrication of metal nanoparticles within p(AN-co-APTMACl) hydrogel, first silver ions were loaded into hydrogel network by dispersing 0.2 g of the dried p(AN-co-APTMACl) hydrogel in 50 mL of 500 ppm aqueous solution of silver acetate for 24 h at room temperature under continuous stirring. Ag(I) ion-containing hydrogels were washed with DI to remove unbound metal ions. Then, to reduced metal ions within hydrogel network, metal ion-containing hydrogels were treated with 50 mL of 0.1 M NaBH₄. Finally, the prepared p(AN-co-APTMACl)-Ag hydrogel composites were filtered, washed with DI and used for characterization, as shown in Scheme 1. The amounts of metal nanoparticles entrapped in hydrogels were calculated by AA measurements after dissolution of metal nanoparticles embedded within p(AN-co-APTMACl) hydrogel by treating with 5 M HNO₃ aqueous solution.

Selected FT-IR (KBr, cm⁻¹): (p(AN-co-APTMACl)-Ag⁺): 3452 (br, s), 3292 (sholder), 3088 (w), 2923 (w), 2855 (w), 2239 (m), 1660 (s), 1564 (s), 1522(w), 1401 (m), 1383 (w), 1270 (w), 1132

(m), 1015 (w), 967 (m), 961 (m), 795 (w), 745 (w), 649 (w), 552 (w).

Selected FT-IR (KBr, cm⁻¹): (p(AN-co-APTMACl)-Ag): 3438 (br, s), 3292 (sholder), 3080 (w), 2923 (w), 2850 (w), 2237 (m), 1655 (s), 1559 (s), 1490(w), 1404 (m), 1263 (w), 1165 (w), 1053 (s), 964 (w), 914 (w), 795 (w), 745 (w), 670 (w).

Swelling behavior of p(AN-co-APTMACl) hydrogel

The swelling experiments for the p(AN-co-APTMACl) hydrogel was carried out in water (at room temperature). Pre-weighted hydrogels were immersed in water and the mass increase was recorded by weighing the soaked hydrogels at certain time intervals after blot drying with filter paper to remove the excess solvent on the surface.

General reduction procedure

The catalytic activity of p(AN-co-APTMACl)-Ag composites was studied for the catalytic reduction of 4-NP. 0.061 g (0.01 M) solution of 4-NP was prepared and added into 50 mL of this solution 0.4 g (0.35 M) of NaBH₄ and stirred at 250 rpm. 0.02 g of hydrogel composite was added as a catalyst into this mixture. About 0.3 mL sample was taken out from reaction mixture at different time intervals and diluted up to 10 times. Then, the progress of the reduction reaction was observed by measuring the absorption maxima at 400 nm by UV-Vis spectrophotometer. Reduction rate constant was calculated by measuring the decrease in intensity of absorption peak at 400 nm. To study the effect of temperature on the rate of reduction of 4-NP, the reduction was carried out at three different temperatures; 25 °C, 40 °C and 60 °C keeping the amount of reactants and catalyst constant. Also, the effect of amount of catalyst was

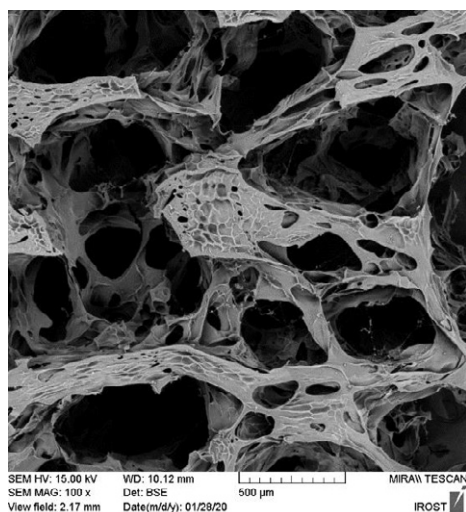


Fig. 1 SEM images of p(AN-co-APTMAcI) hydrogel

investigated on the reduction of 4-NP. For doing so, different amounts of catalysts were used and other reaction conditions were kept constant. To evaluate the reusability of catalysts, after first cycle, the catalysts were separated from the reaction medium by filtration, washed with DI water and used again for the reduction of 4-NP under the same conditions till fourth cycle. All the experiments were repeated at least three times and their average values are given with standard deviations.

General oxidation procedure

A mixture of p(AN-co-APTMAcI)-Ag in water (3.0 mL) was placed into a two-neck flask equipped with a magnetic stirrer. The flask was evacuated and refilled with pure oxygen (balloon filled). Then, the benzyl alcohol (0.108 g, 1.0 mmol) was added into the solution with a syringe. The mixture was heated to reach the set temperature under O_2 atmosphere for 24 h. The resulting mixture was vigorously stirred at 80 °C under O_2 atmosphere for 24 h. After the reaction, the catalyst was de-swelled in CH_2Cl_2 (2.0 mL) for 24 h. Then, the organic phase was analyzed immediately by GC. The oxidation products were identified by comparing the retention times with the literature data. For the blank test with the bare hydrogel without Ag, the oxidation reaction of benzyl alcohol was accomplished with p(AN-co-APTMAcI). To test the reusability of the p(AN-co-APTMAcI)-Ag composite, after every usage, the catalyst was separated from reaction mixture by filtration, washed with DI and reused in the same reaction conditions again.

Hydrolysis of $NaBH_4$ catalyzed by p(AN-co-APTMAcI)-Ag

In the hydrolysis of $NaBH_4$, certain amounts of hydrogel composites containing equal amounts of Ag nanoparticles were placed into 50 mL water at 25 °C. To initiate the hydrolysis reaction, 0.1 M (0.2 g) $NaBH_4$ was added to this reaction mixture and stirred at 1000 rpm. The volume of generated H_2 gas with time was measured in an experimental set up where the produced H_2 gas replaced water in an inverted volumetric cylinder. All the experiments were repeated at least three times and results are given as the averages of these three measurements with their standard deviations. To determine the effect of temperature on $NaBH_4$ hydrolysis and determine the activation parameters, 0.1 g of p(AN-co-APTMAcI)-Ag hydrogel composite was used in $NaBH_4$ hydrolysis at 25, 40 and 60 °C under the same reaction conditions.

RESULTS AND DISCUSSION

Synthesis and Characterization

The characterization of porous p(AMPS) hydrogels and their metal composites were carried out with various characterization techniques, such as SEM images, FT-IR spectroscopy, TEM images and AA spectroscopy.

The structure of p(AMPS) hydrogels was determined using a SEM (JEOL 2010) on thin sections of freeze-dried p(AMPS) hydrogels. The SEM image of p(AMPS), shown in Fig. 1, indicates the formation of homogeneous and highly porous material.

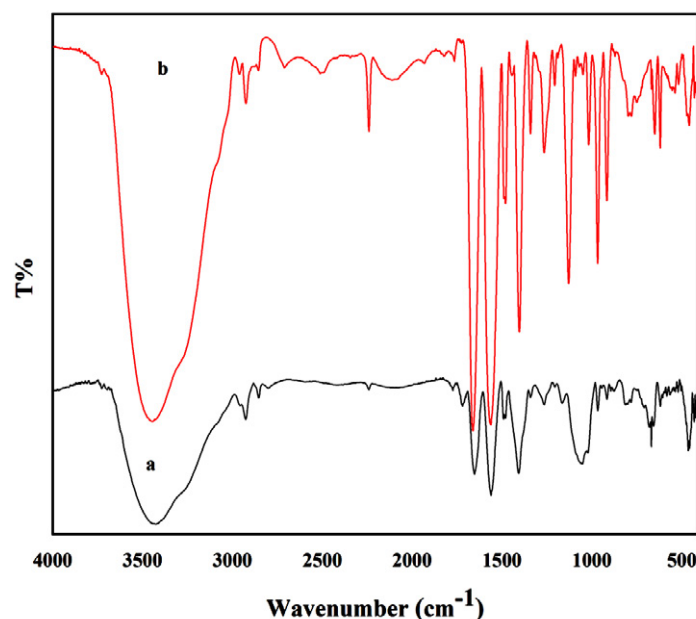


Fig. 2 FT-IR spectra of a) p(AN-co-APTMACl) hydrogel, b) p(AN-co-APTMACl)-Ag composite

To determine the swelling behavior of p(AN-co-APTMACl) hydrogels, distillation water was chosen as the swelling media. The swelling ratios were estimated using the following equation:

$$\text{Swelling ratio (\%)} = (W_s - W_d) / W_d \times 100$$

where W_s is the weight of swollen hydrogel and W_d is the weight of the dried hydrogel at time zero. The swelling percent values of p(AN-co-APTMACl) hydrogel was 2800% in H_2O .

To confirm the functional groups in co-polymeric hydrogels, the FT-IR spectra of hydrogel are presented in Fig. 3a. This figure shows the characteristic of nitrile stretching band originating from AN groups at about 2240 cm^{-1} . The peaks belong to the APTMACl monomer and cross linker at 3292 cm^{-1} and 3072 cm^{-1} for N-H stretching vibrations of the amide group [18]. Additionally, the peaks observed at 2929 cm^{-1} and 2878 cm^{-1} in the spectra of all the hydrogels are related to -CH stretching vibrations, while the peaks at 1665 cm^{-1} are related to the C=O stretching vibrations for p(AN-co-APTMACl) hydrogel. Similarly, the band for N-H bending appeared at 1561 cm^{-1} , and the band at 1490 cm^{-1} clearly shows the existence of an ammonium ion [19-21].

A schematic representation of metal loading and in situ reduction process for the formation of metal nanoparticles inside hydrogel networks is demonstrated in Scheme 1. To investigate the nanostructure of the sample, TEM measurement

was carried out. The TEM images of metal nanoparticles-containing p(AN-co-APTMACl) hydrogels are given in Fig. 3. As seen, metal nanoparticles with a uniform spherical shape, about $<50\text{ nm}$, are distributed within p(AN-co-APTMACl) hydrogel matrices.

The amount of metal ion within the hydrogels was determined using AAS after dissolution by HNO_3 treatment and its amount is 0.0139 mmol/g hydrogel. And finally, the chemical changes in the structure of p(AN-co-APTMACl)-Ag composites were confirmed via FT-IR spectroscopy by recording the FT-IR spectra p(AN-co-APTMACl)-Ag as seen in Fig. 2-b. After loading the Ag ions and reduction to Ag^0 nano-particles, the small shifts in FT-IR spectra of p(AN-co-APTMACl)-Ag are related to interactions between Ag and hydrogel matrix, as shown in Fig. 2-b.

The catalytic activity of p(AN-co-APTMACl)-Ag toward the reduction reaction of 4-nitrophenol

A reduction reaction of the conversion of 4-NP to 4-AP was chosen as a model reaction to evaluate the catalytic activity of the synthesized p(AN-co-APTMACl)-Ag composites. For this purpose, $NaBH_4$ was added as a reducing agent and p(AN-co-APTMACl)-Ag hydrogel composite as a catalyst. It should be noted that conversion of 4-NP to 4-AP cannot be carried out by $NaBH_4$ without assisting any catalyst. According to



Fig. 3 TEM images of metal nanoparticles from p(AN-co-APTMACI)-Ag

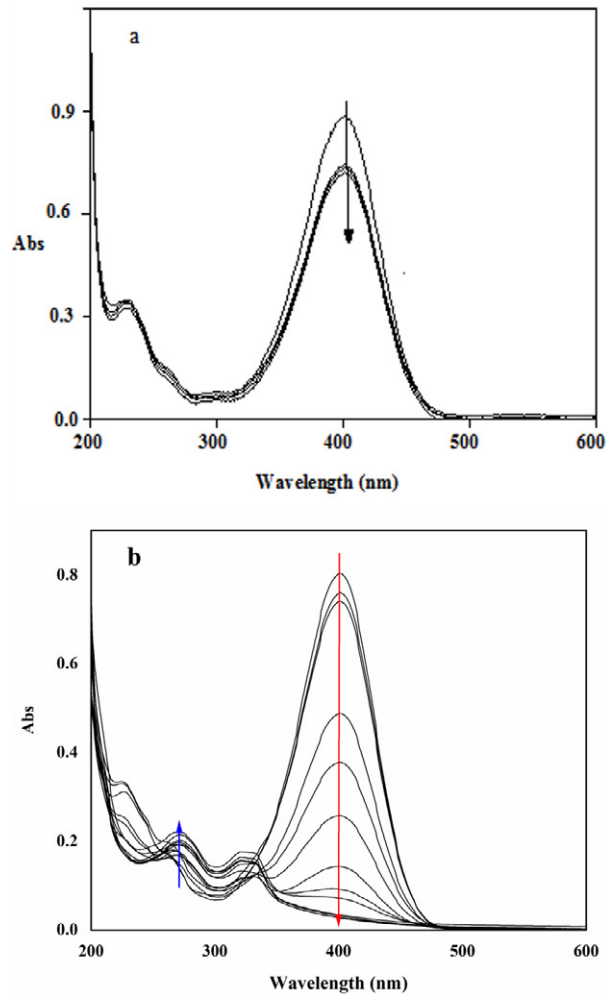


Fig. 4 UV-Vis spectra of 4-NP in the absence of catalyst and presence of NaBH_4 . (b) UV-Vis spectra for the reduction of 4-NP catalyzed by p(AN-co-APTMACI)-Ag composite and NaBH_4 . Reaction conditions; 0.01 M 4-NP 50 mL, $\text{NaBH}_4 = 0.2$ M, catalyst = 27.8 μmol , 25 $^\circ\text{C}$

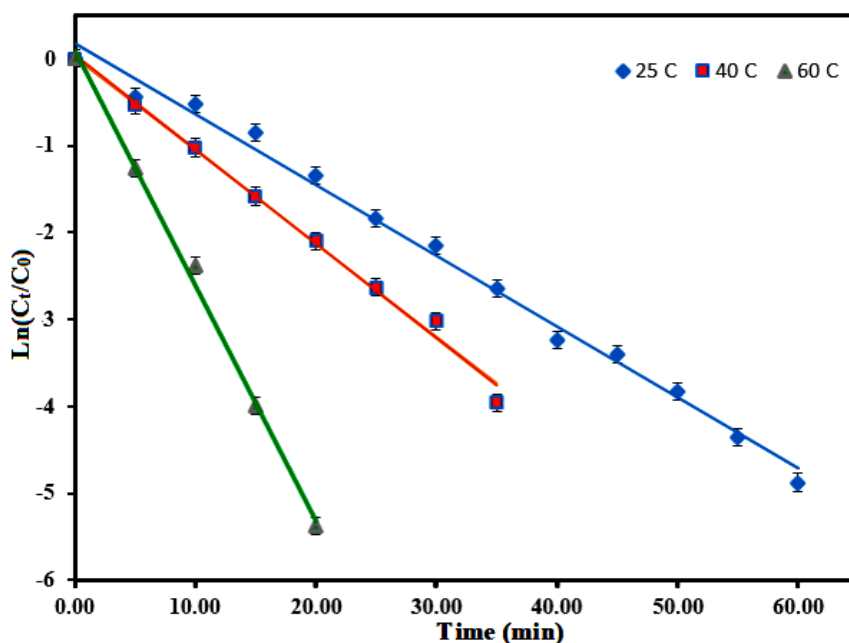


Fig. 5 The determination of apparent rate constants (k_{app}) for the reduction of 4-NP catalyzed by p(AN-co-APTMAcI)-Ag composites with temperature

the thermodynamic studies, the reduction of nitro compounds is possible in the presence of excess amounts of aqueous solution of NaBH_4 , as reducing agent, with a large kinetic barrier [22]. The contribution of a catalyst helps to overcome this energy barrier making these reactions feasible under mild conditions such as room temperature. In all the catalytic reduction of nitro aromatic compounds, 27.8 μmol of hydrogel-Ag composites was used as the catalyst.

Reduction of nitro compound was tracked by measuring the decrease in their absorbance peak in UV-Vis spectra taken at various time intervals. Only a small amount of 4-NP was reduced in the absence of catalyst even after 3 hours, as shown in Fig. 5-a. After addition of catalyst almost all of the 4-NP present in the reaction mixture was reduced within 60 minutes as demonstrated in Fig. 5-b.

As reduction of NP was carried out in a large excess of NaBH_4 so this reaction was supposed to be the pseudo first order and values of k_{app} were calculated by plotting $\ln(C_t/C_0)$ vs. time as shown in Fig. 6. In order to evaluate the effect of temperature on the catalytic activity of p(AMPS)-Ag composite the reduction of 4-NP was investigated in three different temperatures; 25 °C, 40 °C, 60 °C keeping the amount of reactant and catalyst constant. Dependence of reaction rate on temperature is displayed in Fig. 6; $\ln(C_t/C_0)$ versus time at different

temperatures. The reduction rates were increased linearly as temperature increased, because at higher temperature, the rate of diffusion of reactant molecules into hydrogel composites and collision frequency of reactant and catalyst increase due to increase in the average kinetic energy of molecules.

Activation parameters can be calculated from the data obtained by the reduction reactions carried out at different temperatures catalyzed by p(AN-co-APTMAcI)-Ag composite. Energy of activation (E_a) was calculated from the Arrhenius equation, as given in Eq. 1.

$$\ln k = \ln A - (E_a/RT) \quad (1)$$

According to the Arrhenius equation, $\ln k_{app}$ was plotted against $1/T$ as shown in Fig. 7-a, E_a was calculated from the slope of this plot and found to be equal to 28.26 kJ mol^{-1} .

The activation enthalpy (ΔH^\ddagger) and entropy (ΔS^\ddagger) were calculated by using Eyring equations (Eq. (2)).

$$\ln k/T = \ln (k_B/h) + \Delta S^\ddagger/R - \Delta H^\ddagger/R (1/T) \quad (2)$$

According to Eyring equation, $\ln k_{app}/T$ was plotted against $1/T$ as shown in Fig. 7-b. The value of ΔH^\ddagger was calculated from the slope of this plot and was found to be 25.64 kJ mol^{-1} . The positive

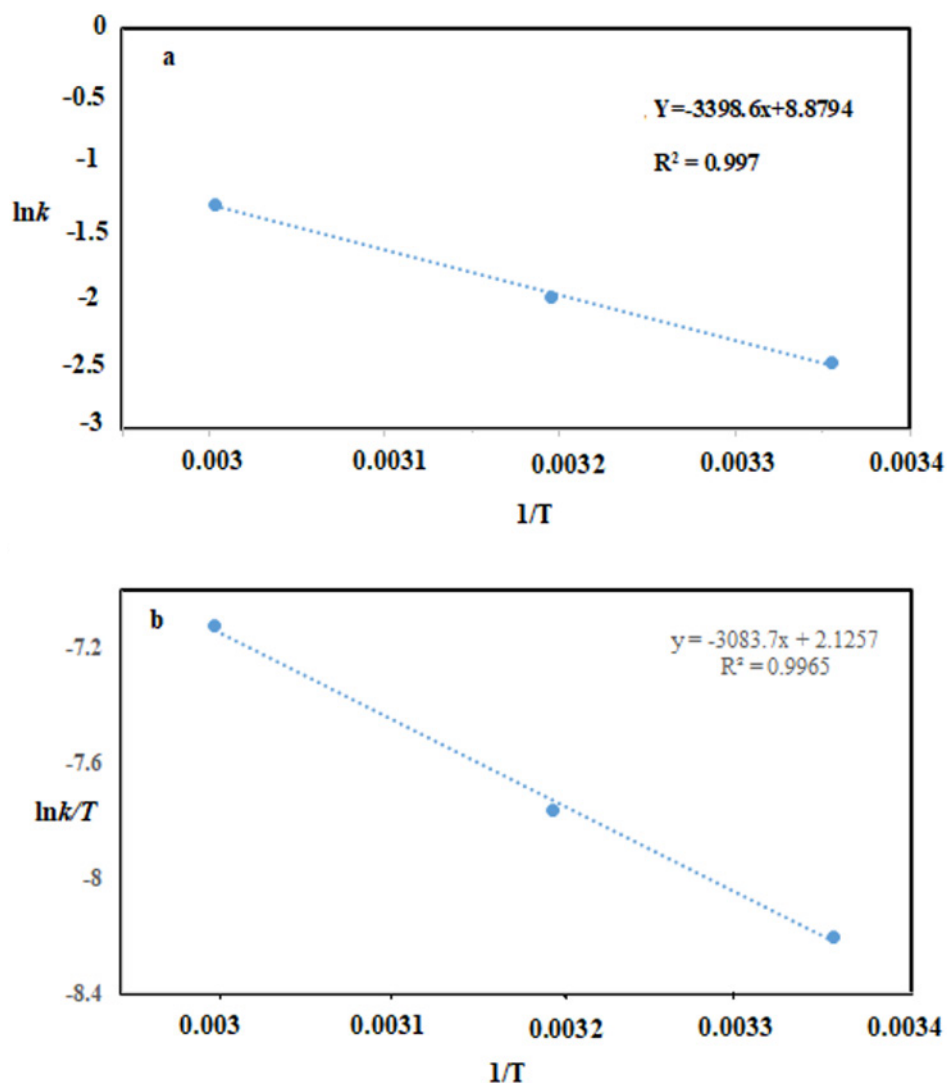


Fig. 6 The determination of apparent rate constants (k_{app}) for the reduction of 4-NP catalyzed by p(AN-co-APTMACl)-Ag with temperature, a) plot of $\ln(k_{app})$ vs. $1/T$, b) plot of $\ln(k_{app}/T)$ vs. $1/T$ for the reduction of 4-NP catalyzed by p(AN-co-APTMACl)-Ag with temperature

value of ΔH^\ddagger shows that the formation of an activated complex in the reduction of 4-NP is an endothermic process [31]. The value of ΔS^\ddagger ($-179.78 \text{ J mol}^{-1} \text{ K}^{-1}$) was calculated from the intercept of plot of $\ln(k_{app}/T)$ vs. $1/T$. The negative value of ΔS^\ddagger shows that the reduction of 4-NP is entropically unfavorable that could become favorable by adding catalyst [23]. The value of ΔG^\ddagger was calculated from the equation $\Delta G^\ddagger = \Delta H^\ddagger - T\Delta S^\ddagger$.

The values of ΔG^\ddagger at 298 K, 313 K and 333 K were calculated as $79.21 \text{ kJ mol}^{-1}$, $81.91 \text{ kJ mol}^{-1}$, and $85.51 \text{ kJ mol}^{-1}$, respectively. The positive values of ΔG^\ddagger shows that reduction of 4-NP is a

non-spontaneous process [24] and it needs an input energy to proceed which is provided by the addition of the catalyst.

The effect of catalyst amount on the reduction rate of 4-NP was also investigated. The reaction was studied at three different amounts of catalyst *viz.* 0.01, 0.02, 0.04 g. As shown in Fig. 7-a, with an increase in catalyst amount, the increase in rate of reaction was observed, as expected. With increasing the amount of catalysts, the available catalytic sites are also increased. According to availability of greater number of catalytic sites, the greater number of reactants are adsorbed on the

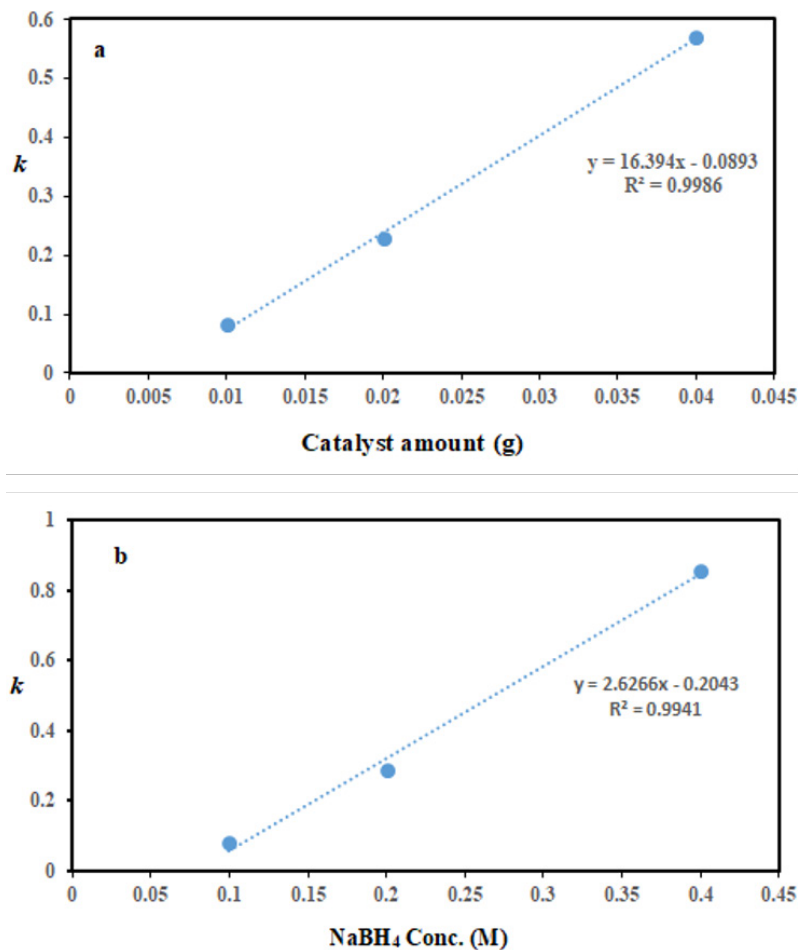


Fig. 7 a) The change in reduction of the rate constant of 4-NP with the amount of Ag catalyst inside p(AN-co-APTMAcI)-Ag composites, and b) change in values of k_{app} with the change in concentration of NaBH_4 during the reduction of NP

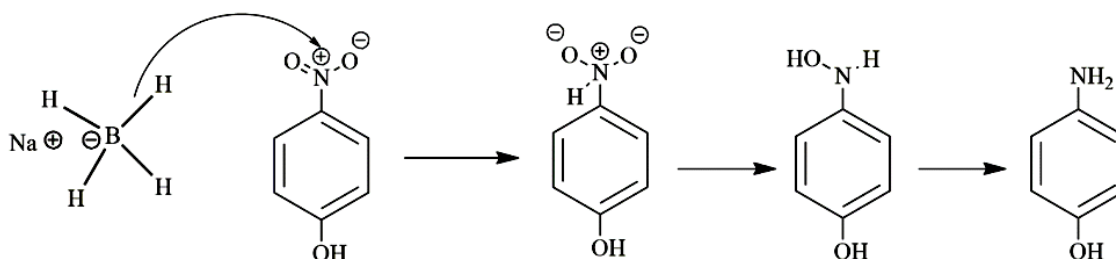
surface of catalyst at the same time, resulting in an increase in rate of the product formation.

In order to investigate the effect of amount of reducing agent on the reduction rate, different amounts of NaBH_4 were used by assuming that all other parameters are constant. For evaluation the effect of NaBH_4 on the reduction rate, different amounts of NaBH_4 (0.1-0.4 M) were used in reduction of 4-NP. As can be seen from Fig. 7-b, there is a linear increase in the reduction rate of 4-NP with the increase in the amount of NaBH_4 at 25 °C. The same trend has been reported in the literature [25].

The reusability of p(AN-co-APTMAcI)-Ag catalyst system was studied by using the same catalyst in 4-NP reduction repeatedly up to four times. After every use, the catalyst was filtered and washed with DI, and reused for the same reaction

under the same reaction conditions without significant loss of activity.

According to literature reports, the reduction of 4-NP to 4-AP at the surface of a nanocatalysts takes place via Langmuir-Hinshelwood mechanism [26]. The proposed mechanism for the reduction of 4-NP at the surface of Ag nanoparticle is schematically shown in Scheme 2. Both the reducing agent and 4-NP react at the surface of Ag nanoparticles fabricated in hydrogel network. When NaBH_4 is added in water, BH_4^- is produced which is a strong nucleophile. Being a strong nucleophile, BH_4^- gives electron to catalyst and produces hydride ion. The hydride ions then react with proton (H^+) provided by water to produce hydrogen molecules (H_2). The H_2 molecules are adsorbed at the surface of Ag nanoparticles. The antibonding orbitals of the H_2 molecules accept



Scheme 2. Mechanism for reduction of 4-NP on the surface of Ag nanoparticles fabricated in p(AN-co-APTMACI) hydrogel

electron pairs from electron flow of catalyst and H_2 molecules are converted into active hydrogen atoms which remain adsorbed at the surface of Ag nanoparticles. The active hydrogen atoms then attack at the nitro group of 4-NP and convert it to 4-AP via formation of intermediates containing nitroso ($-NO$) and hydroxylamino ($-NHOH$) groups as shown by the structural formulas on the surface of Ag nanoparticles in Scheme 2. When 4-AP is formed at the surface of Ag nanoparticles, it is desorbed from the surface of nanoparticle and in this way surface of nanoparticle is regenerated for further action. Desorption of product is followed by the adsorption of new reactant molecules at the surface of catalyst. In this way adsorption-desorption equilibrium is established and reactants are continuously converted into the products [27]. Kinetic of such reactions depends on the rate of diffusion of reactants and products through the hydrogel network [28]. The rate of diffusion further depends on hydrophilicity of hydrogel, porosity of hydrogels and cross linking density of hydrogels. A hydrogel with high hydrophilic nature, greater porosity and low crosslinking density can facilitate easy diffusion of reactants and products and hence can be considered as a suitable milieu for rapid reaction.

H_2 Production by hydrolysis of $NaBH_4$

Finally, metal nanoparticle containing hydrogel composites was used in hydrogen generation reactions from the hydrolysis of $NaBH_4$ under stable reaction conditions of 50 mL 0.1 M $NaBH_4$, at 25 °C. Each hydrolysis reaction in this study was repeated at least three times and the average of these measurements was calculated with standard deviation.



The H_2 generation reactions from hydrolysis

of $NaBH_4$ were performed at three different temperatures to understand the effect of temperature and calculate the activation parameters. It was found that temperature is highly effective on H_2 generation reactions from hydrolysis of $NaBH_4$. The effect of the temperature on the hydrolysis of $NaBH_4$ was determined by using 0.1 g p(AN-co-APTMACI)-Ag metal composites (containing 1.39 μmol nanoparticles) at different temperatures which changed between 25 and 60 °C under certain reaction conditions as given in experimental section. As the temperature of the reaction medium is increased, the times to produce the same amount of H_2 was decreased as demonstrated in Fig. 8. As can be seen, the H_2 generation reaction was completed within about 110 min at 25 °C, whereas the same reaction was completed within about 30 min at 60 °C. The thermodynamic parameters of the hydrolysis reaction of $NaBH_4$ were calculated using the very well-known Arrhenius (Eq. (1)) and Eyring (Eq. (2)) equations associated with the graphs of $\ln k$ versus $1/T$ and $\ln(k/T)$ versus $1/T$ graphs as given in Fig. 9-a and Fig. 9-b, respectively.

As can be seen in Fig. 9, $\ln k$ versus $1/T$ and $\ln(k/T)$ versus $1/T$ provide a good linear relation. However, the activation energy was calculated by applying Eq. (1) for different temperatures, the same data were also used by applying Eq. (2) for calculation of activation enthalpy and entropy. The activation parameters of energy, enthalpy and entropy of p(AMPS)-Ag metal composite systems were determined as $E_a = 24.49 \text{ kJ mol}^{-1}$, $\Delta H^\ddagger = 21.87 \text{ kJ mol}^{-1}$ and $\Delta S^\ddagger = -207.136 \text{ J mol}^{-1} \text{ K}^{-1}$, respectively.

The catalytic activity of p(AN-co-APTMACI)-Ag toward the oxidation reaction of alcohols

The selective oxidation of alcohols, particularly with O_2 as the terminal oxidant, is one of the fundamental and important reactions in organic syntheses [29]. With the p(AN-co-APTMACI)-Ag

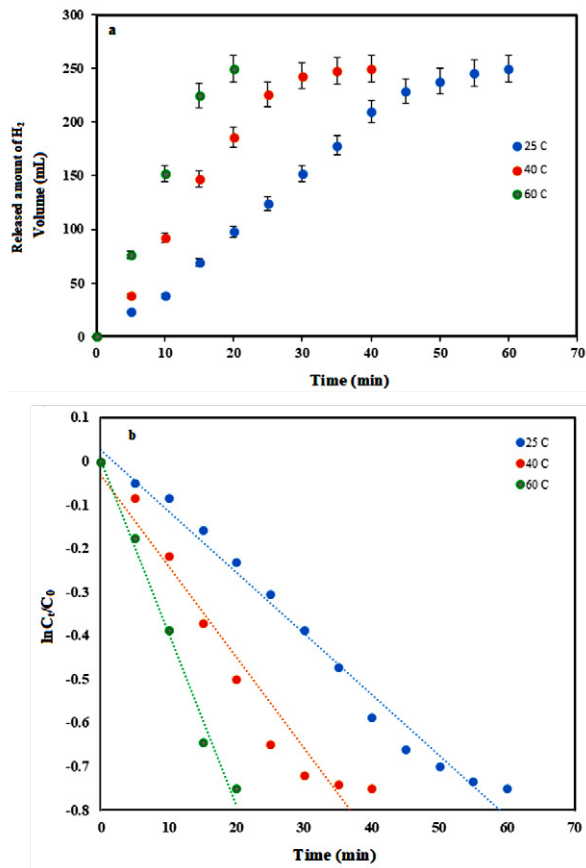


Fig. 8 The effects of temperature on the hydrolysis of NaBH₄, b) ln k versus 1/T (Arrhenius eq., and c) ln (k/T) versus 1/T (Eyring eq.). [50 ml 50 m M NaBH₄, 1.39 μmol Ag in 0.1 g p(AN-co-APTMACI)-Ag hydrogel-metal composite].

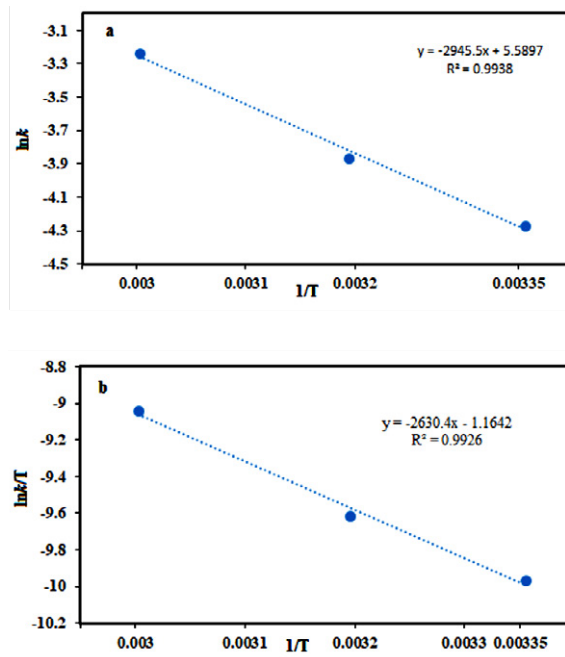


Fig. 9 a) ln k versus 1/T (Arrhenius eq.), and (b) ln (k/T) versus 1/T (Eyring eq.)

Table 1. Catalytic activity of p(AN-co-APTMAcI)-Ag on the oxidation of benzyl alcohol ^a

Entry	Substrate	Catalyst amount g catalyst (μmol Ag)	Conversion ^b (%)	Product	Selectivity (%)
1		0.01 g (13.9)	21		>99
2		0.02 g (27.8)	54		>99
3		0.02 g (27.8)	72		>99
4		0.02 g (27.8)	36		>99
5		0.02 g (27.8)	23		>99

^a Catalyst (0.02 g), substrate (1.0 mmol), H₂O, (5 mL) as solvent, K₂CO₃ 1.2 mmol, temperature 80 °C, Time = 24 h under O₂ atmosphere. ^c Conversions are based on the starting substrate.

catalyst in hand, we aim to evaluate its catalytic activity for the aerobic oxidation of alcohols, and some results are summarized in Table 1.

In the beginning, the oxidation reaction of the benzyl alcohol as the model substrate was performed in water at 80 °C. The blank experiments without Ag loading exhibits a negligible benzyl alcohol conversion (<7% at 60 °C and 24 h reaction time). However, in the presence of the Ag catalyst, benzyl alcohol conversion increases. Within 24 h and with 0.0025 g catalyst (0.011 mmol Ag), 75.5% isolated yield of the benzoic acid was acquired. Within 24 h and with 0.005 g catalyst (0.022 mmol Ag), 95.4% isolated yield of the benzoic acid was obtained (Table 1, entries 1-2).

Encouraged by these promising results, we then directed our attention toward the oxidation of other primary benzyl alcohols with substituent such as 4-MeO, 4-NO₂ and 4-Cl groups (Table 1, entries 3-5). Carboxylic acids and aldehyde as products were observed for 4-MeO substrates investigated but for other substrates carboxylic acid as sole product was observed. The substitution

effect on aromatic substrates was studied. As shown in Table 1, the conversion of alcohols increased in the presence of electron-donating substituent, such as -OMe at the *para*- position of benzyl alcohol, (Table 1, entry 3), but in contrast, withdrawing group, such as NO₂ and Cl (Table 1, entries 4-5) decreased the conversion [30,31]. This trend is in accordance with Hammett plot results, suggesting that the formation of the transition state with a carbocationic character on the benzylic carbon during the discharge of hydrogen in the rate-determining step is involved in the oxidation pathway over the present catalysts [32].

CONCLUSION

In this study, the p(AN-co-APTMAcI)-Ag composites were prepared, and the related hydrogels were obtained in the presence of APTMAcI and AN monomers. p(AN-co-APTMAcI) was successfully utilized for the in situ synthesis of Ag NPs within the gel matrix. This is a facile and convenient green chemical approach to make a gel-based nanohybrid system, in which the Ag NPs are almost uniformly

fabricated. The as-prepared Ag NPs containing the p(AN-co-APTMA/Cl) hybrid gel could be explored within the catalysis of an organic reaction using a green chemical approach. These heterogeneous catalysts were readily available and easy to handle as they are stable in air. Reuse of the catalysts can be achieved without loss in their activity.

ACKNOWLEDGEMENTS

Authors are thankful to University of Zanjan for financial support of this study.

CONFLICT OF INTEREST

There is no conflict of interest.

REFERENCES

- Pó R. Water-Absorbent Polymers: A Patent Survey. *Journal of Macromolecular Science, Part C: Polymer Reviews*. 1994;34(4):607-62.
- Dudu TE, Sahiner M, Alpaslan D, Demirci S, Aktas N. Removal of As(V), Cr(III) and Cr(VI) from aqueous environments by poly(acrylonitril-co-acrylamidopropyl-trimethyl ammonium chloride)-based hydrogels. *Journal of Environmental Management*. 2015;161:243-51.
- Xu G, Gao S, Ji X, Zhang X. Characterization and Synthesis Mechanism of Nanosilver/PAMPS Composites by Microwave. *Soft Nanoscience Letters*. 2014;04(02):15-23.
- Caló E, Khutoryanskiy VV. Biomedical applications of hydrogels: A review of patents and commercial products. *European Polymer Journal*. 2015;65:252-67.
- Thakur A, Wanchoo R, Singh P. Structural parameters and swelling behavior of pH sensitive poly (acrylamide-co-acrylic acid) hydrogels. *Chemical and Biochemical Engineering Quarterly*. 2011;25(2):181-94.
- Merino S, Martín C, Kostarelos K, Prato M, Vázquez E. Nanocomposite Hydrogels: 3D Polymer-Nanoparticle Synergies for On-Demand Drug Delivery. *ACS Nano*. 2015;9(5):4686-97.
- Murali Mohan Y, Vimala K, Thomas V, Varaprasad K, Sreedhar B, Bajpai SK, et al. Controlling of silver nanoparticles structure by hydrogel networks. *Journal of Colloid and Interface Science*. 2010;342(1):73-82.
- Bilginyay R, Khan F, Mann S. Spontaneous patterning and nanoparticle encapsulation in carboxymethylcellulose/alginate/dextran hydrogels and sponges. *Materials Science and Engineering: C*. 2010;30(3):352-6.
- Cong H-P, Yu S-H. Self-assembly of functionalized inorganic-organic hybrids. *Current Opinion in Colloid & Interface Science*. 2009;14(2):71-80.
- Ghorbanloo M, Moharramkhani N, Yazdely TM, Monfared HH. Cationic hydrogel and graphene oxide based cationic hydrogel with embedded palladium nanoparticles in the aerobic oxidation of olefins. *Journal of Porous Materials*. 2018;26(2):433-41.
- Mauter MS, Elimelech M. Environmental Applications of Carbon-Based Nanomaterials. *Environmental Science & Technology*. 2008;42(16):5843-59.
- Soppimath KS, Aminabhavi TM, Kulkarni AR, Rudzinski WE. Biodegradable polymeric nanoparticles as drug delivery devices. *Journal of Controlled Release*. 2001;70(1-2):1-20.
- Desimone MF, Hélyary C, Rietveld IB, Bataille I, Mosser G, Giraud-Guille M-M, et al. Silica-collagen bionanocomposites as three-dimensional scaffolds for fibroblast immobilization. *Acta Biomaterialia*. 2010;6(10):3998-4004.
- Van Vlierberghe S, Dubrue P, Schacht E. Biopolymer-Based Hydrogels As Scaffolds for Tissue Engineering Applications: A Review. *Biomacromolecules*. 2011;12(5):1387-408.
- Tang Z, Gao L, Wu Y, Su T, Wu Q, Liu X, et al. BSA-rGO nanocomposite hydrogel formed by UV polymerization and in situ reduction applied as biosensor electrode. *Journal of Materials Chemistry B*. 2013;1(40):5393.
- Kelly JA, Shukaliak AM, Cheung CCY, Shopsowitz KE, Hamad WY, MacLachlan MJ. Responsive Photonic Hydrogels Based on Nanocrystalline Cellulose. *Angewandte Chemie*. 2013;125(34):9080-4.
- Cao J, Cai Y, Yu L, Zhou J. Dual physically crosslinked hydrogels based on the synergistic effects of electrostatic and dipole-dipole interactions. *Journal of Materials Chemistry B*. 2019;7(4):676-83.
- Sahiner N, Ilgin P. Synthesis and characterization of soft polymeric nanoparticles and composites with tunable properties. *Journal of Polymer Science Part A: Polymer Chemistry*. 2010;48(22):5239-46.
- Ozay O, Aktas N, Sahiner N. Hydrogels as a Potential Chromatographic System: Absorption, Speciation, and Separation of Chromium Species from Aqueous Media. *Separation Science and Technology*. 2011;46(9):1450-61.
- Sahiner N, Singh M, De Kee D, John VT, McPherson GL. Rheological characterization of a charged cationic hydrogel network across the gelation boundary. *Polymer*. 2006;47(4):1124-31.
- Sahiner N, Demir S, Yildiz S. Magnetic colloidal polymeric ionic liquid synthesis and use in hydrogen production. *Colloids and Surfaces A: Physicochemical and Engineering Aspects*. 2014;449:87-95.
- Ajmal M, Siddiq M, Al-Lohedan H, Sahiner N. Highly versatile p(MAC)-M (M: Cu, Co, Ni) microgel composite catalyst for individual and simultaneous catalytic reduction of nitro compounds and dyes. *RSC Adv*. 2014;4(103):59562-70.
- Genç F, Uzun C, Güven O. Quaternized poly(1-vinylimidazole) hydrogel for anion adsorption. *Polymer Bulletin*. 2015;73(1):179-90.
- Sahiner N, Yildiz S, Al-Lohedan H. The resourcefulness of p(4-VP) cryogels as template for in situ nanoparticle preparation of various metals and their use in H₂ production, nitro compound reduction and dye degradation. *Applied Catalysis B: Environmental*. 2015;166-167:145-54.
- Butun S, Sahiner N. A versatile hydrogel template for metal nano particle preparation and their use in catalysis. *Polymer*. 2011;52(21):4834-40.
- Begum R, Rehan R, Farooqi ZH, Butt Z, Ashraf S. Physical chemistry of catalytic reduction of nitroarenes using various nanocatalytic systems: past, present, and future. *Journal of Nanoparticle Research*. 2016;18(8).
- Farooqi ZH, Khan SR, Begum R. Temperature-responsive hybrid microgels for catalytic applications: a review. *Materials Science and Technology*. 2016;33(2):129-37.

28. Khan SR, Farooqi ZH, Waheed uz Z, Ali A, Begum R, Kanwal F, et al. Kinetics and mechanism of reduction of nitrobenzene catalyzed by silver-poly(N-isopropylacryl amide-co-allylacetic acid) hybrid microgels. *Materials Chemistry and Physics*. 2016;171:318-27.
29. He X, Chen L, Zhou X, Ji H. Recyclable Pd supported catalysts with low loading for efficient epoxidation of olefins at ambient conditions. *Catalysis Communications*. 2016;83:78-81.
- [30] Sharma PD, Panchariya P, Purohit P, Sharma PK. Structure-reactivity correlation in the oxidation of substituted benzyl alcohols by imidazolium fluorochromate. *European Chemical Bulletin*. 2013;2(10):816-24.
31. Ghorbanloo M, Nosrati Fallah H. Silver nanoparticle embedded anionic crosslinked copolymer hydrogels: an efficient catalyst. *Journal of Porous Materials*. 2020;27(3): 765-77.
32. Harada T, Ikeda S, Hashimoto F, Sakata T, Ikeue K, Torimoto T, et al. Catalytic Activity and Regeneration Property of a Pd Nanoparticle Encapsulated in a Hollow Porous Carbon Sphere for Aerobic Alcohol Oxidation. *Langmuir*. 2010;26(22):17720-5.